# Microscopic Origin of the Effective Spin-Spin Interaction in a Semiconductor Quantum Dot Ensemble

Frederik Vonhoff, Andreas Fischer, Kira Deltenre, and Frithjof B. Anders
*Department of Physics, Technical University Dortmund, Otto-Hahn-Straße 4, 44227 Dortmund, Germany*

(Received 1 July 2022; accepted 19 September 2022; published 11 October 2022)

We present a microscopic model for a singly charged quantum dot (QD) ensemble to reveal the origin of the long-range effective interaction between the electron spins in the QDs. Wilson's numerical renormalization group (NRG) is used to calculate the magnitude and the spatial dependency of the effective spin-spin interaction mediated by the growth-induced wetting layer. Surprisingly, we found an antiferromagnetic Heisenberg coupling for very short inter-QD distances that is caused by the significant particle-hole asymmetry of the wetting layer band at very low filling. Using the NRG results obtained from realistic parameters as input for a semiclassical simulation for a large QD ensemble, we demonstrate that the experimentally reported phase shifts in the coherent spin dynamics between single- and two-color laser pumping can be reproduced by our model, solving a long-standing open problem of the microscopic origin of the inter-QD electron spin-spin interaction.

DOI: 10.1103/PhysRevLett.129.167701

Spins confined in semiconductor quantum dots (QDs) have been discussed as candidates for the implementation of quantum bits (qubits) in quantum information technologies [1–3], since it allows integration into conventional semiconductor logic elements. While superconducting qubits are on the rise, the first semiconductor QD devices with two qubits were realized only a few years ago [4,5] and are still in the early stages of development. A general understanding of inter-QD spin interactions in semiconductors is essential for further development [6,7]. For information processing, qubit initialization and readout [8,9] are as important as manipulations of the spins. Optical control experiments in QD ensembles [10,11] as well as the measurements of the dephasing time as a function of the laser spectral width [12] in such samples provided strong evidence for long-range electron spin-spin interactions between the different QDs in the ensemble of unknown microscopic origin.

It was speculated [10] that it might be caused by an optically induced [13] Ruderman-Kittel-Kasuya-Yosida (RKKY) interaction [14–16]. Since the laser pulse duration is on the order of picoseconds, such an optically induced interaction, however, would decay rather rapidly and is not compatible with the observed spin coherence on a scale of several nanoseconds. This has remained a long-standing open problem for the last ten years. In order to make use of the intrinsic long-range spin-spin interaction between the localized spins in QDs by spin manipulation protocols [1], its origin needs to be understood.

In this Letter, we propose a microscopic mechanism based on the analysis of a multi-impurity Anderson model [17–19]. We start from a localized electron-bound state in each QD that weakly hybridizes with the conduction band (CB) of the thin wetting layer (WL) [20–22] that is left below the QDs in the Stranski-Krastanow growth protocol. The basic setup is sketched in Fig. 1. By including all virtual charge fluctuations in the leading order, significant corrections to the conventional textbook expression starting from an effective local moment picture have been reported [17,23] for short distances. We believe that implementing back gates below the WL would allow one to manipulate the properties of the low concentration WL electron gas and hence to control the effective spin-spin interaction.

Recently a growth procedure for InGaAs QD ensembles was proposed [24] to eliminate the WL. In such samples, the effective spin-spin interaction between the QD electron spins should be absent. While those types of QD ensembles are produced to decrease the energy loss when used as photon emitters, a detailed investigation of their spin properties in electron-doped samples is still missing to the best of our knowledge.

*Model.*—The WL is treated as a free two-dimensional CB

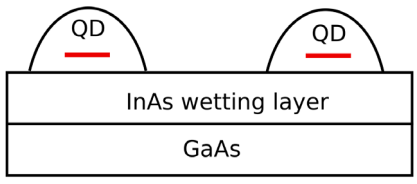


FIG. 1. Sketch of two quantum dots that are linked by the InAs wetting layer.

 

$$H_{\mathrm{WL}} = \sum_{\vec{k}} \frac{\hbar^2 \vec{k}^2}{2m^*} c^\dagger_{\vec{k}\sigma} c_{\vec{k}\sigma} \tag{1}$$

in the isotropic effective mass approximation with $m^*/m_0 = 0.023$ [25]. The minimal model for the $N_{\mathrm{QD}}$ QDs in the ensemble is given by

$$H_{\mathrm{QD}} = \sum_i^{N_{\mathrm{QD}}} \left( \sum_\sigma \varepsilon_i^d d^\dagger_{i\sigma} d_{i\sigma} + U_i n^d_{i\uparrow} n^d_{i\downarrow} \right), \tag{2}$$

where $\varepsilon_i^d$ denotes the single-particle energy of the bound electron state with spin $\sigma$ in the $i$th QD and $U_i$ is the corresponding Coulomb repulsion preventing the bound state to be doubly occupied. The creation (annihilation) operator $d^\dagger_{i\sigma}(d_{i\sigma})$ adds (removes) an electron to (from) the $i$th QD. The electronic wave function is localized but covers the whole diameter of the QD. The parameters $U_i$ and $\varepsilon_i^d$ depend on the individual shape of the QD. Using the experimental estimates [26], we approximate $U_i \approx 4$ meV for a QD with a diameter $d_{\mathrm{QD}} = 25$ nm.

The concentration of the donors in the QD ensemble used in Ref. [10] was selected to match the QD density in the sample. Each QD can capture at least one electron if the bound state energy $\varepsilon_i^d$ is below the CB of the WL. It remains empty when the chemical potential $\mu < \varepsilon_i^d$. Spin spectroscopy experiments [27], however, indicate that not all QDs are filled with one electron. This might be due to local imperfections that shift individual $\varepsilon_i^d$ to higher energies. Also doubly occupied QD states are possible when $\varepsilon_i^d < \mu - U_i$. Excluding this doubly occupied QD ground state configuration puts a lower bound on $\varepsilon_i^d$. We assume that a fraction $q_{\mathrm{WL}}$ of the total donor excess electrons is filling up the WL such that the chemical potential $\mu > 0$ lies within the CB of the WL. The upper bound of the chemical potential $\mu = \varepsilon_F$ is reached for $q_{\mathrm{WL}} = 1$ yielding $\varepsilon_F \approx 1$ meV for a dot density of $10^{10}$ cm$^{-2}$ [10].

The bound state of the $i$th QD can tunnel with a finite tunneling amplitude $V^i_m$ into the Wannier orbital $m$ of the WL. The resulting hybridization term between the bound state of each QD and the WL takes the form

$$H_{\mathrm{hyb}} = \sum_{i=1}^{N_{\mathrm{QD}}} \sum_\sigma \sum_m (V^i_m d^\dagger_{i\sigma} c_{m\sigma} + \mathrm{H.c.}), \tag{3}$$

where $c_{m\sigma}$ is the annihilation operator of the Wannier orbital at site $\vec{R}_m$ of the 2D WL and whose spatial Fourier transform is $c_{\vec{k}\sigma}$. The total Hamiltonian of the coupled QD problem is given by $H = H_{\mathrm{WL}} + H_{\mathrm{QD}} + H_{\mathrm{hyb}}$, which is just a realization of a multi-impurity problem [18].

The effect of the WL on the dynamics of the localized QD states is determined by the hybridization function matrix [17,18]

$$\Delta_{ij}(z) = \sum_{lm} \frac{1}{N} \sum_{\vec{k}} \frac{[V^i_l]^* V^j_m e^{i\vec{k}(\vec{R}_m - \vec{R}_l)}}{z - \varepsilon_{\vec{k}}}. \tag{4}$$

In the wideband limit, i.e., $V_0/D \ll 1$, where $D$ is the bandwidth of the WL CB, $t_{ij} = \mathrm{Re}\Delta_{ij}(\mu)$ generates an effective hopping between the QDs $i$ and $j$. The averaged distance between the QDs is of the same order of magnitude as the Fermi wavelength $\lambda_F$. The distance variations between the WL sites, however, are small compared to $\lambda_F$. Consequently, we can replace $\vec{R}_m - \vec{R}_l$ by the distance between the two centers of the QDs, i.e., $\vec{R}_i - \vec{R}_j$, and include the spatial extension of the QD [28] by defining $\bar{V}_i = \sum_m V^i_m$. We introduce the average hybridization matrix element $V_0^2 = \langle \bar{V}_i^2 \rangle$ and define a reference energy scale $\Gamma_0 = \pi V_0^2 \rho_0$, $\rho_0$ being the constant density of state of the 2D WL CB. The charge fluctuation scale $\Gamma_0$ determines the order of magnitude of $\Delta_{ij}(z)$. The antiferromagnetic (AF) part of the RKKY interaction can be estimated [17,18] as $J^{\mathrm{RKKY}}_{\mathrm{AF},ij} \approx 4t_{ij}^2/U \propto 4\Gamma_0^2/U$ serving as a first estimate for $\Gamma_0 \approx 10 - 100$ $\mu$eV.

In a conventional metal, the chemical potential is located roughly in the middle of the band continuum, and $D > \bar{J}_K$, $U > \bar{J}_K$ holds. $\bar{J}_K$ denotes the averaged local Heisenberg coupling between the QD electron spin and the local CB spin density [29], and local moments are well defined due to large Coulomb interaction. Since in our case $\bar{J}_K > U$, the conventional perturbation theory fails. Additionally, the energy $\varepsilon_i^d$ is located below the lower band edge of the CB, and the chemical potential must be small to allow for a local moment formation.

*Numerical renormalization group approach.*—To circumvent the inconsistency problem of the conventional two-stage perturbative approach, where first the charge fluctuations are eliminated and then in a second step the effective interaction between the local moments is calculated, we apply the numerical renormalization group (NRG) [30,31] to the Hamiltonian with $N_{\mathrm{QD}} = 2$ to determine the distance-dependent effective Heisenberg interaction between the localized electron spins. For each distance $R = |\vec{R}_1 - \vec{R}_2|$, the two-QD problem is mapped onto an effective two-band model [17,32,33], where we used $\Gamma_0$, $\mu = \varepsilon_F$, and $\varepsilon_i^d = \varepsilon^d$ as the adjustable parameters such that each QD remains singly charged. Note that the NRG mapping of the strongly asymmetric bands onto a Wilson chain [30,31,34] leads to a modification of the hopping parameters (see Supplemental Material [35]) and of the NRG fixed point spectrum [40].

Using the NRG, we calculated the temperature-dependent spin-spin correlation function $\langle \vec{S}_1 \vec{S}_2 \rangle(T, R)$ as shown for two distances in Fig. 2(a). The sign of $\langle \vec{S}_1 \vec{S}_2 \rangle(T, R)$ determines the sign of $J_{12}^{\mathrm{RKKY}}(R)$, and $|J_{12}^{\mathrm{RKKY}}(R)|$ is obtained from the fit to the universal functions of the spin-spin correlation function of a model comprising two

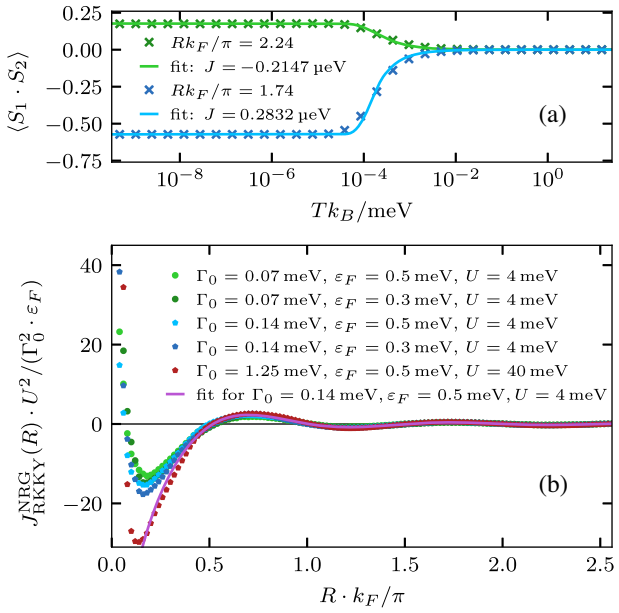


FIG. 2. NRG results: (a) $\langle \vec{S}_1 \vec{S}_2 \rangle(T, R)$ vs $T$ for two distances $R$ and the fit to an interacting two-spin model for extracting $J$. (b) $J^{\text{NRG}}_{\text{RKKY}}(R)/(\Gamma_0^2 \varepsilon_F)$ vs $Rk_F/\pi$ for different $\Gamma_0$ and $\varepsilon_F$. We added a fit to Eq. (5) as the solid magenta line. The graphs corresponding to $U = 4$ meV are calculated with $\epsilon^d = -1.5$ meV, the red graph corresponding to $U = 40$ meV with $\epsilon^d = -15$ meV. NRG parameters $\Lambda = 5$, high energy cutoff $D = 1$ eV and $\bar{\beta} = 40$.

spins $s = 1/2$ coupled by an effective Heisenberg interaction $J$, $S_{12}(T) = -\mu_{\text{eff}}^2(1 - e^{-\beta J})/(1 + 3e^{-\beta J})$, where the parameter $\mu_{\text{eff}}^2$ includes possible Kondo screening effects of the localized spins [41]. We added the fit functions as solid lines to Fig. 2(a). The extracted $J_{12}^{\text{RKKY}}(R)$ are shown in Fig. 2(b) for different fixed sets of parameters.

For two localized moments coupled by a Heisenberg interaction $J_K$ to the local spin-density of 2D CB with a quadratic dispersion in 2D, Fischer and Klein [29] derived the analytic expression

$$J_{ij}^{\text{RKKY}} = -\rho_0 \bar{J}_K^2 \frac{\bar{v} k_F^2}{4\pi} [J_0(k_F R) N_0(k_F R) + J_1(k_F R) N_1(k_F R)] \tag{5}$$

for the effective RKKY interaction, where $J_l(x)$ $[N_l(x)]$ is the Bessel [Neumann] function of order $l$ and $\bar{v}$ is the area of the 2D unit cell. We added a fit to expression (5) to our NRG data as a solid magenta line in Fig. 2(b). The NRG results follow excellently the analytic predictions for larger distances. The magnitude of $J_{ij}^{\text{RKKY}}$ is proportional to $\Gamma_0^2 \varepsilon_F$ as expected, but the absolute value differs from that predicted by Eq. (5). The coupling $J_{ij}^{\text{RKKY}}(R)$ remains invariant under rescaling $\alpha\Gamma_0$, $\alpha U$, and $\alpha\epsilon^d$ for $Rk_F/\pi > 0.5$. For short distances, $Rk_F/\pi < 0.25$, however, we observe significant deviations: The NRG reveals an AF RKKY interaction contrary to the conventional RKKY result. The origin of this surprising effect can be linked to the large effective single-particle hopping between the QD orbitals [42] induced by the very strong particle-hole asymmetry of the CB for small WL fillings. In the literature, a diverging AF RKKY interaction was derived by Proetto and López [43] for $R \to 0$ contradicting the analytical results of Žitko and Bonča [23] predicting a FM coupling. It turns out that the system is close to quantum phase transition for $R = 0$ [42] where the chemical potential $\mu$ governs the transition between an AF and a FM RKKY interaction (see Supplemental Material [35]).

*Spin polarization in laser pulsed QD ensembles.*—After establishing the distance-dependent effective interaction between the electron spins in the different QDs, we investigate its influence on an ensemble of singly charged QDs in an external magnetic field subject to a two-color laser pumping with circularly polarized light [10]. We used a semiclassical simulation [44–46] for the spin dynamics of a QD ensemble model [12]

$$H_{\text{array}} = \sum_i^{N_{\text{QD}}} H_1^{(i)} + \sum_{i<j} J_{ij} \vec{S}^{(i)} \vec{S}^{(j)}, \tag{6}$$

where the central spin model $H_1^{(i)}$,

$$H_1^{(i)} = g_e^{(i)} \mu_B \vec{B}_{\text{ext}} \vec{S}^{(i)} + \sum_{k=1}^{N_i} g_{N,k}^{(i)} \mu_N \vec{B}_{\text{ext}} \vec{I}_k^{(i)} + \sum_{k=1}^{N_i} A_k^{(i)} \vec{I}_k^{(i)} \vec{S}^{(i)}, \tag{7}$$

includes the electron and nuclear Zeeman term in the external magnetic field $\vec{B}_{\text{ext}}$ as well as the hyperfine coupling between the $N_i$ nuclei spins denoted by $\vec{I}_k^{(i)}$ and the electron spin $\vec{S}^{(i)}$ [47–51]. We generated random 2D ensembles of $N_{\text{QD}}$ QDs with a dot density of $10^{10}$ cm$^{-2}$ [10] and assigned $J_{ij} = x_i x_j J^{\text{NRG}}_{\text{RKKY}}(R, \varepsilon_F, \Gamma_0)$ from the NRG data depicted in Fig. 2(b), where $x_i$ accounts for the variations of $\bar{V}_i$. We attributed $N_{\text{QD}}/2$ randomly selected QDs to be resonant to one of the two different laser frequencies and, therefore, also assigned the corresponding $g_e^{(i)}$. We set the average $\bar{g}_e = 0.55$, the ratios between the two subsets $g_e^1/g_e^2 = 1.03$, and $z = \bar{g}_e \mu_B/(\bar{g}_N \mu_N) = 1/800$.

We run three different types of semiclassical simulations for the spin dynamics with $I_k = 3/2$ nuclear spins: (i) a box model with $A_k = A_0 = \text{const}$, $N_{\text{QD}} = 10\,000$, and $N_i = 10^6$ nuclear spins, (ii) a simulation for a frozen nuclear spin dynamics (FOA) [48] for $N_{\text{QD}} = 10\,000$ and $N_i$ as in (i), and (iii) an $A_k$ distribution with $N_{\text{QD}} = 1000$ and $N_i = 1000$ including the full nuclear spin dynamics. In all cases, we kept the characteristic energy scale $T^* = [\sum_k (A_k^{(i)})^2 \langle I_k^2 \rangle]^{-1/2} = 1$ ns fixed. The technical aspects of

the simulation including the treatment of the laser pulse using a trion excitation cycle can be found in the literature [12,45].

The experiments reported in Ref. [10] were performed in a transversal magnetic field of 1 T, and laser pulses of two different colors were applied pumping two different resonant QD subsets. In order to reproduce one of the experimental key results, we first determined a reference curve for $\langle S_z(t)\rangle$ of subset 1 subjected to a circularly polarized laser pulse at $t = 0$ that shows damped coherent oscillations characterized by the Larmor frequency, see the black curve in Fig. 3(a). Then we run the same setup, but apply a second circularly polarized laser pulse with a color resonating with subset 2 at a moment when $\langle S_z(t)\rangle$ of subset 1 reached a minimum, i.e., at a delay of $\Delta t \approx 0.115$ ns.The incident time of the second laser pulse is indicated by a black dot in Fig. 3(a). Clearly visible is that the second trace of $\langle S_z(t)\rangle$ plotted as a blue curve coincides with the reference curve for $t < 0.115$ ns and then starts to acquire a relative phase shift as a function of $\Delta t$ with respect to the reference curve. Therefore, the phase shift is zero up for $t < \Delta t$.

We tracked the relative phase shift $\phi$ of the coherent oscillations between the reference curve and those in the presence of a laser pulse onto subset 2,

$$\phi(t) = \arctan\left(\frac{S_z^{(1)}}{S_y^{(1)}}\right) - \arctan\left(\frac{S_{\mathrm{Ref},z}^{(1)}}{S_{\mathrm{Ref},y}^{(1)}}\right). \tag{8}$$

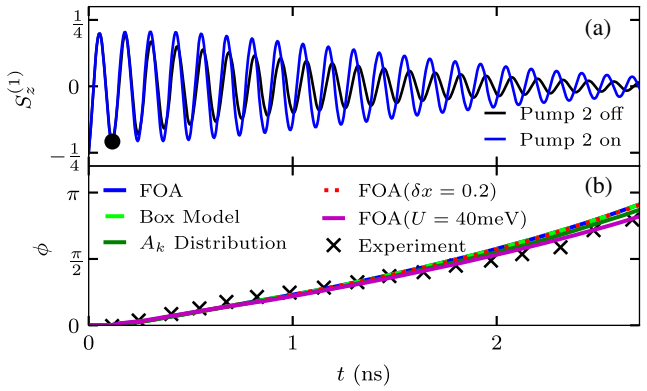


FIG. 3. Semiclassical simulation of the QD ensemble. (a) Traces of the electron spin dynamics using the frozen Overhauser field approximation (FOA) with $\Gamma_0 = 0.14$ meV, $\epsilon^d = -1.5$ meV, and $U = 4$ meV. A phase shift $\phi$ in the coherent electron spin oscillations between a single-color pumping reference curve and a two-color laser pumped QD ensemble occurs. The incidence time of the second pump is marked as a black circle. (b) Comparison of the experimental phase shift $\phi$ to various simulations. The simulations are for a FOA, for $A_k = \mathrm{const}$ (box model), a distribution of the $A_k$, including some disorder of the $x_j$ as well as the second set of parameters with $\Gamma_0 = 1.25$ meV, $\epsilon^d = -15$ meV, and $U = 40$ meV. The experimental data are taken from Ref. [10].

The sign of the phase shift depends only on the relative sign of the circular polarization. The result is plotted in Fig. 3(b). As in the experiment, the phase shift increases roughly linearly in time. The slope is determined by the overall magnitude of $J_{ij}^{\mathrm{RKKY}}(R)$. The results that resemble the experiments very well were obtained for $\Gamma_0 = 140$ $\mu$eV and $\varepsilon_F = 0.5$ meV corresponding to $q_{\mathrm{WL}} = 0.5$ and $U/\Gamma_0 = 29$. The order of magnitude of $J_{ij}^{\mathrm{RKKY}}(R)$ is determined by the ratio $(\Gamma_0/U)^2$, indicating that the physics is driven by an effective local Kondo coupling [52]. Leaving the ratio $U/\Gamma_0 = 29$ fixed, we can also reproduce the experimental phase shifts with $\Gamma_0 = 1.25$ meV, $\epsilon^d = -15$ meV, and $U = 40$ meV and confirm the main scaling property. Note that the individual hybridization strength between the bound electron QD state and the local Wannier orbital remains small and is of the order $V_m^i = 10$–$40$ $\mu$eV. Only by the summation to $\bar{V}_i$, a significant contribution arises.

We run the simulation for fixed $x_i = 1$ and for the FOA additional with a Gaussian normal distribution with $\delta x = 0.2$ to reveal the influence of the local derivation of the QD hybridization matrix element from its average value. The phase shifts are nearly independent of the distribution of local hybridization matrix elements $\bar{V}_i$. The major disorder contributions stem from the random distribution of distances to the neighboring QDs. As a result, each QD senses a slightly different effective coupling, converting the quadratic increase of the phase shift in a two-QD model to a linear increase for short times. Tracking the full dynamics of the Overhauser field is not required on the time scale of 3 ns: The frozen Overhauser approximation and the case $A_k^{(i)} = A_0$ yield the almost same results as the full nuclear spin dynamics, but with a reduced $N_{\mathrm{QD}}$. We also run the simulation for a $J_{ij}^{\mathrm{RKKY}}(R)$ after rescaling $\Gamma_0$, $U$, and $\epsilon^d$ with a factor of 10 to accommodate for errors in the rough parameter estimates. The slope of the phase shift $\phi$ came out about 50% too large, requiring a reduction of $\Gamma_0$. The origin of the increase is caused by the contribution of the first minimum in $J_{ij}^{\mathrm{RKKY}}(R)$ at around $RK_F/\pi \approx 0.2$, where we observe significant deviations from the analytic prediction. Overall, the simulation data agree remarkably well with the experimental findings even over a large range of parameters.

*Conclusion.*—In this Letter, we present a QD WL model to explain the microscopic origin of the inter-QD electron spin-spin interaction conjectured in Ref. [10]. We used Wilson's NRG [31] to extract the strength and distance dependency of this spin-spin interaction mediated by the WL via an a RKKY-based mechanism. While the long-distance behavior is in agreement with the low-filling perturbative RKKY result [29], we found significant deviations for shorter distances. The unconventional AF RKKY interaction at short distances can be connected to the large effective inter-QD hopping between the QD

orbitals [17,18,42] as a consequence of the very low band filling. The conventional RKKY approach [29] starts already from an effective local moment picture and does not include all corrections in $O(V_0^4)$.

We used our NRG data as input for a semiclassical simulation of the spin dynamics in a coupled QD ensemble, which is able to reproduce the experimental phase shifts reported for a two-color pumping setup [10] very accurately for a variety of different realistic parameters. Although the interaction in the effective model might appear substantial, one has to bare in mind that all WL Wannier orbitals below a QD contribute in Eq. (3) only by a very weak coupling.

Our theory solves the open problem about the microscopic origin of the inter-QD spin-spin interaction, which remained unsolved for over ten years [10]. We predict that this interaction can be eliminated by a QD growth process that excludes an InAs WL [24]. By gating the 2D WL, it might be possible to modulate the 2D electron gas and, therefore, control the effective Heisenberg interactions $J_{ij}^{\mathrm{RKKY}}(R)$ by a change of gate voltage.

The authors would like to thank Alex Greilich for fruitful discussions, who also provided the experimental raw data of Ref. [10] added to Fig. 3(b). We acknowledge financial support by the Deutsche Forschungsgemeinschaft through the transregio TRR 160 within the Projects No. A4 and No. A7, and the computing time granted by the John von Neumann Institute for Computing (NIC) under Project No. HDO09 at the Jülich Supercomputing Centre.

[1] D. Loss and D. P. DiVincenzo, Quantum computation with quantum dots, Phys. Rev. A **57**, 120 (1998).
[2] F. P. G. de Arquer, D. V. Talapin, V. I. Klimov, Y. Arakawa, M. Bayer, and E. H. Sargent, Semiconductor quantum dots: Technological progress and future challenges, Science **373**, 640 (2021).
[3] R. Hanson, L. P. Kouwenhoven, J. R. Petta, S. Tarucha, and L. M. K. Vandersypen, Spins in few-electron quantum dots, Rev. Mod. Phys. **79**, 1217 (2007).
[4] M. Veldhorst, C. H. Yang, J. C. C. Hwang, W. Huang, J. P. Dehollain, J. T. Muhonen, S. Simmons, A. Laucht, F. E. Hudson, K. M. Itoh, A. Morello, and A. S. Dzurak, A two-qubit logic gate in silicon, Nature (London) **526**, 410 (2015).
[5] T. F. Watson, S. G. J. Philips, E. Kawakami, D. R. Ward, P. Scarlino, M. Veldhorst, D. E. Savage, M. G. Lagally, M. Friesen, S. N. Coppersmith, M. A. Eriksson, and L. M. K. Vandersypen, A programmable two-qubit quantum processor in silicon, Nature (London) **555**, 633 (2018).
[6] X. Zhang, H.-O. Li, G. Cao, M. Xiao, G.-C. Guo, and G.-P. Guo, Semiconductor quantum computation, Natl. Sci. Rev. **6**, 32 (2018).
[7] X. Xue, T. F. Watson, J. Helsen, D. R. Ward, D. E. Savage, M. G. Lagally, S. N. Coppersmith, M. A. Eriksson, S. Wehner, and L. M. K. Vandersypen, Benchmarking Gate Fidelities in a Si/SiGe Two-Qubit Device, Phys. Rev. X **9**, 021011 (2019).
[8] J. M. Elzerman, R. Hanson, L. H. W. van Beveeren, B. Witkamp, L. M. K. Vandersypen, and L. P. Kouvenhoven, Single-shot read-out of an individual electron spin in a quantum dot, Nature (London) **430**, 431 (2004).
[9] M. Atatüre, J. Dreiser, A. Badolato, A. Högele, K. Karrai, and A. Imamoglu, Quantum-dot spin-state preparation with near-unity fidelity, Science **312**, 551 (2006).
[10] S. Spatzek, A. Greilich, S. E. Economou, S. Varwig, A. Schwan, D. R. Yakovlev, D. Reuter, A. D. Wieck, T. L. Reinecke, and M. Bayer, Optical Control of Coherent Interactions between Electron Spins in InGaAs Quantum Dots, Phys. Rev. Lett. **107**, 137402 (2011).
[11] S. Varwig, A. René, S. E. Economou, A. Greilich, D. R. Yakovlev, D. Reuter, A. D. Wieck, T. L. Reinecke, and M. Bayer, All-optical tomography of electron spins in (In,Ga)As quantum dots, Phys. Rev. B **89**, 081310(R) (2014).
[12] A. Fischer, E. Evers, S. Varwig, A. Greilich, M. Bayer, and F. B. Anders, Signatures of long-range spin-spin interactions in an (In,Ga)As quantum dot ensemble, Phys. Rev. B **98**, 205308 (2018).
[13] C. Piermarocchi, P. Chen, L. J. Sham, and D. G. Steel, Optical RKKY Interaction between Charged Semiconductor Quantum Dots, Phys. Rev. Lett. **89**, 167402 (2002).
[14] M. A. Ruderman and C. Kittel, Indirect exchange coupling of nuclear magnetic moments by conduction electrons, Phys. Rev. **96**, 99 (1954).
[15] T. Kasuya, A theory of metallic ferro- and antiferromagnetism on Zener's model, Prog. Theor. Phys. **16**, 45 (1956).
[16] K. Yosida, Magnetic properties of Cu-Mn alloys, Phys. Rev. **106**, 893 (1957).
[17] F. Eickhoff, B. Lechtenberg, and F. B. Anders, Effective low-energy description of the two-impurity Anderson model: RKKY interaction and quantum criticality, Phys. Rev. B **98**, 115103 (2018).
[18] F. Eickhoff and F. B. Anders, Strongly correlated multi-impurity models: The crossover from a single-impurity problem to lattice models, Phys. Rev. B **102**, 205132 (2020).
[19] F. Eickhoff and F. B. Anders, Kondo holes in strongly correlated impurity arrays: RKKY-driven Kondo screening and hole-hole interactions, Phys. Rev. B **104**, 045115 (2021).
[20] S. Sanguinetti, K. Watanabe, T. Tateno, M. Wakaki, N. Koguchi, T. Kuroda, F. Minami, and M. Gurioli, Role of the wetting layer in the carrier relaxation in quantum dots, Appl. Phys. Lett. **81**, 613 (2002).
[21] R. V. N. Melnik and M. Willatzen, Bandstructures of conical quantum dots with wetting layers, Nanotechnology **15**, 1 (2003).
[22] S. Lee, O. L. Lazarenkova, P. von Allmen, F. Oyafuso, and G. Klimeck, Effect of wetting layers on the strain and electronic structure of InAs self-assembled quantum dots, Phys. Rev. B **70**, 125307 (2004).
[23] R. Žitko and J. Bonča, Multiple-impurity anderson model for quantum dots coupled in parallel, Phys. Rev. B **74**, 045312 (2006).
[24] M. C. Löbl, S. Scholz, I. Söllner, J. Ritzmann, T. Denneulin, A. Kovács, B. E. Kardynał, A. D. Wieck, A. Ludwig, and

R. J. Warburton, Excitons in InGaAs quantum dots without electron wetting layer states, Commun. Phys. **2**, 93 (2019).
[25] *Semiconductors—Basic Data*, edited by O. Madelung (Springer, Berlin, Heidelberg, 1996).
[26] D. Goldhaber-Gordon, H. Shtrikman, D. Mahalu, D. Abusch-Magder, U. Meirav, and M. Kastner, Kondo effect in a single-electron transistor, Nature (London) **391**, 156 (1998).
[27] P. Glasenapp, D. S. Smirnov, A. Greilich, J. Hackmann, M. M. Glazov, F. B. Anders, and M. Bayer, Spin noise of electrons and holes in (In,Ga)As quantum dots: Experiment and theory, Phys. Rev. B **93**, 205429 (2016).
[28] We checked that by an explicit calculation assuming a Gaussian distribution of $V_m^i$ centered at $\vec{R}_j$ with a width given by the QD radius of $r_{\mathrm{QD}} \approx 15$ nm.
[29] B. Fischer and M. W. Klein, Magnetic and nonmagnetic impurities in two-dimensional metals, Phys. Rev. B **11**, 2025 (1975).
[30] H. R. Krishna-murthy, J. W. Wilkins, and K. G. Wilson, Renormalization-group approach to the Anderson model of dilute magnetic alloys. I. Static properties for the symmetric case, Phys. Rev. B **21**, 1003 (1980).
[31] R. Bulla, T. A. Costi, and T. Pruschke, The numerical renormalization group method for quantum impurity systems, Rev. Mod. Phys. **80**, 395 (2008).
[32] B. A. Jones and C. M. Varma, Study of Two Magnetic Impurities in a Fermi Gas, Phys. Rev. Lett. **58**, 843 (1987).
[33] I. Affleck, A. W. W. Ludwig, and B. A. Jones, Conformal-field-theory approach to the two-impurity Kondo problem: Comparison with numerical renormalization-group results, Phys. Rev. B **52**, 9528 (1995).
[34] K. G. Wilson, The renormalization group: Critical phenomena and the Kondo problem, Rev. Mod. Phys. **47**, 773 (1975).
[35] See Supplemental Material at http://link.aps.org/supplemental/10.1103/PhysRevLett.129.167701 for more details on the NRG implementation and for a demonstration of how the change of $\mu$ induces a change between an AF and a FM RKKY interaction for $R \to 0$, which includes the Refs. [36–39].
[36] M. Yoshida, M. A. Whitaker, and L. N. Oliveira, Renormalization-group calculation of excitation properties for impurity models, Phys. Rev. B **41**, 9403 (1990).
[37] R. Bulla, N.-H. Tong, and M. Vojta, Numerical Renormalization Group for Bosonic Systems and Application to the Sub-Ohmic Spin-Boson Model, Phys. Rev. Lett. **91**, 170601 (2003).
[38] R. Bulla, H.-J. Lee, N.-H. Tong, and M. Vojta, Numerical renormalization group for quantum impurities in a bosonic bath, Phys. Rev. B **71**, 045122 (2005).
[39] R. Žitko and T. Pruschke, Energy resolution and discretization artifacts in the numerical renormalization group, Phys. Rev. B **79**, 085106 (2009).
[40] R. Hager, Kondo-Effekt in Systemen mit niedriger Ladungsträgerkonzentration, Master's thesis, Department of Physics, University of Augsburg, 2007.
[41] $\mu_{\mathrm{eff}}^2 = s(s+1)$ for unscreened spins.
[42] T. Esat, B. Lechtenberg, T. Deilmann, ChristianWagner, P. Krüger, R. Temirov, M. Rohlfing, F. B. Anders, and F. S. Tautz, A chemically driven quantum phase transition in a two-molecule Kondo system, Nat. Phys. **12**, 867 (2016).
[43] C. Proetto and A. López, Magnetic exchange interactions in cerium compounds, Phys. Rev. B **25**, 7037 (1982).
[44] M. M. Glazov and E. L. Ivchenko, Spin noise in quantum dot ensembles, Phys. Rev. B **86**, 115308 (2012).
[45] N. Jäschke, A. Fischer, E. Evers, V. V. Belykh, A. Greilich, M. Bayer, and F. B. Anders, Nonequilibrium nuclear spin distribution function in quantum dots subject to periodic pulses, Phys. Rev. B **96**, 205419 (2017).
[46] A. Fischer, I. Kleinjohann, N. A. Sinitsyn, and F. B. Anders, Cross-correlation spectra in interacting quantum dot systems, Phys. Rev. B **105**, 035303 (2022).
[47] M. Gaudin, Diagonalisation d'une classe d'hamiltoniens de spin, J. Phys. **37**, 1087 (1976).
[48] I. A. Merkulov, A. L. Efros, and M. Rosen, Electron spin relaxation by nuclei in semiconductor quantum dots, Phys. Rev. B **65**, 205309 (2002).
[49] W. A. Coish and D. Loss, Hyperfine interaction in a quantum dot: Non-Markovian electron spin dynamics, Phys. Rev. B **70**, 195340 (2004).
[50] W. Zhang, V. V. Dobrovitski, K. A. Al-Hassanieh, E. Dagotto, and B. N. Harmon, Hyperfine interaction induced decoherence of electron spins in quantum dots, Phys. Rev. B **74**, 205313 (2006).
[51] G. Chen, D. L. Bergman, and L. Balents, Semiclassical dynamics and long-time asymptotics of the central-spin problem in a quantum dot, Phys. Rev. B **76**, 045312 (2007).
[52] J. R. Schrieffer and P. A. Wolff, Relation between the Anderson and Kondo Hamiltonians, Phys. Rev. **149**, 491 (1966).